2007

Industrial robot track modeling and vibration suppression

Tao, WeiMin; Zhang, MingFun; Ma, Ou; Yu, XiaoPing

Monterey, California; Naval Postgraduate School

Industrial Robot: An International Journal 34/4 (2007) 317325 q Emerald Group Publishing Limited [ISSN 0143-991X]
http://hdl.handle.net/10945/38263

Research article

Industrial robot track modeling and vibration suppression

WeiMin Tao
Brooks Automation Inc., Palo Alto, California, USA

MingJun Zhang
Agilent Technologies, Palo Alto, California, USA

Ou Ma
New Mexico University, Las Cruces, New Mexico, USA, and

XiaoPing Yun
Naval Postgraduate School, Monterey, California, USA

Abstract
Purpose – The purpose of this paper is to investigate the vibration suppression of industrial track robot and propose a practical solution.
Design/methodology/approach – Root-cause analysis through dynamic modeling, and vibration suppression using the acceleration smoother.
Findings – The vibration is due to insufficient damping based on the model analysis. The solution achieved significant performance improvement without redesign of robot hardware and controller.
Research limitations/implications – The design of the proposed acceleration smoother is still empirical based, which is unable to achieve optimal design.
Practical implications – This solution is very easy to implement. It is robust, reliable and is able to generate consistent results.
Originality/value – A very practical industrial solution, especially useful for upgrading the existing systems in the field without redesign the hardware and controller.

Keywords Robotics, Control systems, Modeling, Vibration

Paper type Research paper

Introduction

The track axis for industrial robot studied in this paper is shown in Figure 1. It is often used in semiconductor and microarray fabrication industries for wafer handlings. The robot is a selective compliant articulated robot arm (SCARA) robot mounted on a linear track. Rapid point-to-point motion for the robot track is usually involved in manufacturing environment. To transfer a wafer from one point to another, the robot track needs to go through a series of motions involving start – acceleration – constant-speed – deceleration – stop. Abrupt changes in acceleration or deceleration will result in vibrations at the robot's end-effector that holds a wafer. The vibration may cause wafer slippery and long settling time, which is undesirable for industrial manufacturing applications.

The current issue and full text archive of this journal is available at
www.emeraldinsight.com/0143-991X.htm

Industrial Robot: An International Journal
34/4 (2007) 317–325

[DOI 10.1108/01439910710749645]

It is important to understand the dynamics involved in the process and to develop efficient methods to suppress the vibration for such robot tracks. To do that, it is crucial to create and study its basic mathematical model. In this paper, a dynamic model for this type of robot tracks will be first presented. A solution for vibration suppression will then be proposed. The particular modeling provides a good reference for similar industrial robot tracks. The generic solution for vibration suppression can be easily applied to other applications.

The robot track in this paper refers to the track system with SCARA robot as a payload. The track is driven by a DC motor with a gear ratio for power transmission. The robot is mounted on a robot platform connected to the track motor through a few pulleys and timing belts.

By suppressing the vibration of the robot track, the vibration of robot's end-effector can be significantly reduced. Below is a brief summary of the main approaches to reduce or eliminate the vibrations of robotic and control systems:

- Increase damping by structural design or adding dampers: to ensure large damping, high natural frequency and stiffness (Kim and Hong, 2004; Roy and Whitcomb, 1999).

Figure 1 An industrial robot track

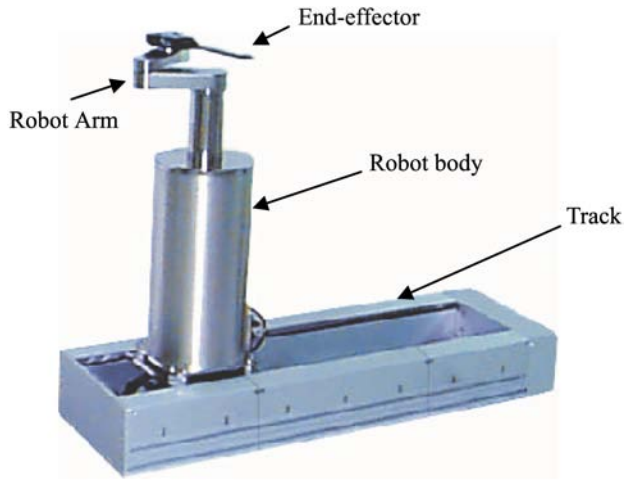

- Open loop approaches: including trajectory smoothing, input shaping and feed-forward approaches. The typical trajectory smoothing approaches (e.g. S-curve motion profiling) employ a multi order polynomial time equation to compute trajectory output (Lambrechts *et al.*, 2004; Meckl and Seering, 1985) with variable velocity profiles (e.g. second order for trapezoidal and third order for S-curve). These approaches reduce the vibration by generating a smooth trajectory, which also accounts for the electrical saturation characteristics of the motor amplifier. Input shaping approach convolves a sequence of impulses to produce a shaped input as the motion command. It reduces residual vibration by generating an input that cancels its own vibration (Singhose *et al.*, 1994; Singer and Seering, 1990; Singhose and Singer, 1996; Murphy and Watanabe, 1992). Feed-forward approaches typically make use of input and model information to generate control output and to make the plant follow the predefined vibration free trajectory (Piazzi and Visioli, 2000; Kim and Hong, 2004). The open-loop approaches have to work with close-loop control to achieve other control objectives such as steady-state accuracy, system stability and robustness against disturbances and uncertainties, etc.
- Close-loop approaches, such as conventional PID control, adaptive PID control, model-based adaptive control (McEver and Leo, 2001; Coyle-Byrne and Klafter, 1990; Whitcomb *et al.*, 1993; Book *et al.*, 1976), H_∞ control design (Doyle *et al.*, 1989), etc.

The trajectory smoothing approach is one of the most popular approaches currently used in robotic industry. This is mainly due to its simplicity, flexibility and universality. PID feedback control is a primitive and robust robot control approach, which is easy to implement and can provide satisfactory control performance for varied dynamic characteristics. Other approaches may require accurate models, additional sensors, and/or intensive computations.

In this paper, the PID control and a generic motion profile (S-curve) are used in the control of robot tracks to meet general application requirements. The selection of PID control approach is due to its robustness and simplicity. The selection of S-curve trajectory smoothing approach is, in addition to other benefits mentioned above, because the PID approach fails to tune the system to critical damping ratio, which is crucial for eliminating or reducing the vibration. This failure is mainly due to the implementation constraints, such as tracking error limit, electrical noise, etc. The current control scheme is able to meet most practical requirements. However, for some applications that require smooth track motion with very high motion speed, the existing motion profile and control parameters failed to achieve an acceptable vibration suppression performance. The goal of this study is to resolve such an industrial problem by analyzing the root-cause of the vibration problem and providing a practical and robust solution to the application.

This paper provides an insight of the system performance by modeling and system identification, which reveals the root-cause of the vibration and the limitation of the current system. In addition to the analysis, a practical solution without redesign of the control system is proposed and implemented in the real system, which results in significant performance improvement.

The rest of this paper is organized as follows. In the second section, a mathematical model of the inherent dynamics of the robot track is presented. Third section determines the model parameters through direct measurement and experiments. Fourth section computes the model parameters using system identification approach. Fifth section provides the root-cause analysis based on the given model and root *locus* approach. Sixth section proposes a practical solution for suppressing the vibration. The testing results with two robots are presented in the seventh section. Eighth section concludes the discussion.

Modeling of the industrial robot track

Figure 2 shows a schematic drawing of the robot track system, where a SCARA robot is used as a payload.

The robot track plant includes a SCARA robot, a platform for mounting the robot, a track-driving system. The track-driving system consists of three pulleys, two belts and the track motor. A track belt connects the robot platform and pulley 2. Pulleys 2 and 1 is directly connected by a solid steel shaft. Pulleys 1 and 0 (motor pulley) is connected by a timing belt. Pulley 0 and an encoder are mounted on motor shaft.

For the modeling convenience and without losing the generality, this paper assumes:

Figure 2 A Schematic drawing of the robot track

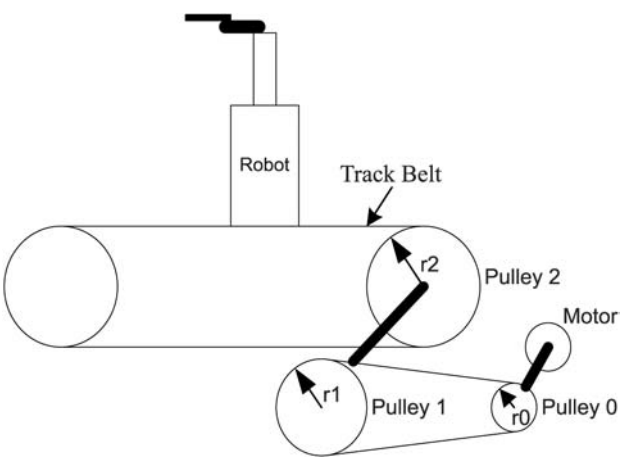

- The track is only subject to motor torque, damping friction and static friction.
- Non-linearity factors are ignored except static friction.
- The belt spring impact is ignored due to negligible belt elongation. Testing data also verified this since the encoder data on the motor shaft and laser data on the robot platform shown almost identical robot motion displacement on the track axis.

Let:
- θ_0, θ_1, θ_2 be rotational angles of motor pulleys 0-2.
- I_0, I_1, I_2 be rotational inertia of motor pulleys 0-2.
- c_0, c_1, c_2, c_m be dynamic coefficients of motor pulley 0, pulley 1/pulley 2 and track trail.
- r_0, r_1, r_2 be radius of motor pulleys 0-2.
- M_{m} be the motor torque.
- M_{f} be the static friction torque.
- m be the weight of robot plus robot platform.

For pulley rotation motion, we have following relations:

$$\theta_2 = \theta_1; \quad r_1\theta_1 = r_0\theta_0$$

$v = r_2\dot{\theta}_2$, where, v is the track speed.

The kinetic energy of the system can be expressed as:

$$K = \frac{1}{2}\, mr_2^2\left(\frac{r_0}{r_1}\right)^2\dot{\theta}_0^2 + \frac{1}{2}(I_2 + I_1)\left(\frac{r_0}{r_1}\right)^2\dot{\theta}_0^2 + \frac{1}{2}\, I_0\dot{\theta}_0^2 \qquad (1)$$

Since, the belt spring impact is negligible, the potential energy of the system along the track axis is $P = 0$.

The Rayleigh dissipation (RD) function is:

$$\mathrm{RD} = \frac{1}{2}\left[c_m r_2^2\left(\frac{r_0}{r_1}\right)^2 + (c_2 + c_1)\left(\frac{r_0}{r_1}\right)^2 + c_0\right]\dot{\theta}_0^2 \qquad (2)$$

Define the generalized coordinate as $\theta = \theta_0$ and the external torque M as the sum of motor torque M_{m} and static friction torque M_{f}. By applying Lagrange's equation, the robot track plant equation can be written as follows:

$$a_1\ddot{\theta} + a_2\dot{\theta} = M \qquad (3)$$

where:

$$a_1 = I_0 + (I_1 + I_2)\left(\frac{r_0}{r_1}\right)^2 + mr_2^2\left(\frac{r_0}{r_1}\right)^2 \qquad (4)$$

$$a_2 = c_0 + (c_1 + c_2)\left(\frac{r_0}{r_1}\right)^2 + c_m r_2^2\left(\frac{r_0}{r_1}\right)^2 \qquad (5)$$

$$M = M_{\mathrm{m}} + M_{\mathrm{f}}$$

$$M_f = -m_f\mathrm{Sign}(\dot{\theta})$$

m_{f} is the average static friction value.

In equation (3), a_1 and a_2 can be regarded as lumped rotational inertial and damping friction coefficient on motor shaft. They can be calculated by direct physical data measurement.

From equation (3), the transfer function of θ/M can be written as:

$$G(s) = \frac{\theta}{M} = \frac{1}{S(a_1 S + a_2)} \qquad (6)$$

The above transfer function is only for robot track plant. To model the whole system, we need to consider both the robot plant and the control system, which consists of DAC/amplifier module, encoder and PID controller. Figure 3 shows the track system block diagram with the control system.

Parameter determination

The respective parameters are as follows:
- DAC: 16 b D/A conversion with voltage range of ± 10 V. The DAC gain is 0.0003.
- Amplifier: current gain = 10/7 (A/V).
- Motor: torque constant = 16.8/16 (lb in./A).
- Encoder: encoder gain = 636.62 (count/rad).
- Proportional gain: KP = 320; derivative gain: KD = 0.96; integral gain: KI = 1.5.
- The ratio of track distance and encoder count = 0.57755 (mil/count).
- Other physical parameters are listed below.

Static friction

The static friction was measured through "Breakaway" test. The "Breakaway" approach slowly increases the track torque until the track starts to move. The torque recorded at the moment the track starts to move is considered as static friction. Figure 4 shows the track's static friction with respect to the track location (torque was recorded one point per inch). Notice that the static friction is not constant along the track length. To simplify the model, it is averaged to get the constant static friction.

The average static friction for two motion directions is: 0.56 lb in. for forward motion; 0.76 lb in. for backward motion. The overall average static friction is: $m_{\mathrm{f}} = 0.66$ (lb in.). The Coulomb friction is assumed approximately the same as static friction.

Overall inertial a_1

Applying the data in Table I to formula (4), we can calculate a_1 from direct data measurement:

$$a_1 = 0.0291\ (\mathrm{lb\,in.\,s^2})$$

Damping coefficient a_2

Since, c_i $(i = 0, 1, 2, m)$ are difficult to obtain from direct measurement, a_2 was computed through damping friction measurement, which was conducted with a constant speed motion.

According to equation (3), the damping friction for zero acceleration is the sum of motor torque and static friction:

$$M = M_{\mathrm{m}} + M_{\mathrm{f}}$$

Figure 5 shows the motor torque plots with a slow speed (5,000 counts/s) motion.

The acceleration phase ends after 7,000 encoder counts, and after that the robot moves approximately with a constant speed. The motor torque shows less variation in constant speed phase. An average torque minus static torque is considered as damping friction.

The average motor torque is taken the average between 10,000 and 12,000 counts where the torque noise is relatively smaller:

Figure 3 The block diagram of robot track system

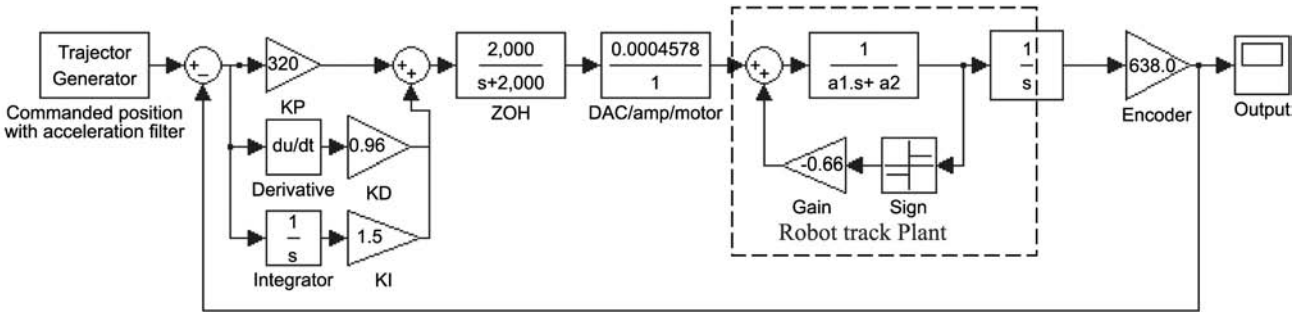

Figure 4 Static friction plots

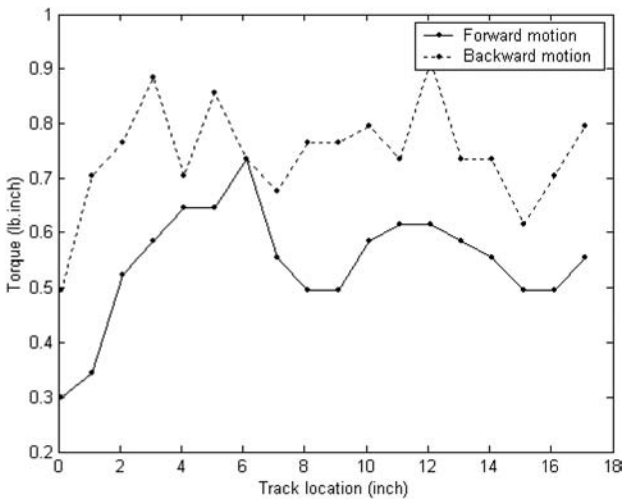

Figure 5 Motor torque plot

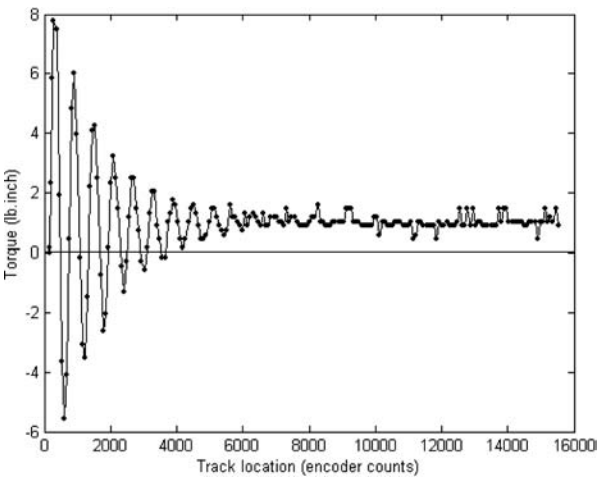

Table I Physical parameters of the robot track

Variable	Unit	Value
m	lb	68
r_0	in.	0.4425
r_1	in.	1.52
r_2	in.	1.263
I_0	lb in. s^2	0.00187
I_1	lb in. s^2	0.00125
I_2	lb in. s^2	0.00125

$$M_m = 0.901 \text{ (lb in.)}$$

The damping friction is: $M = M_m + M_f = 0.241$ (lb in.)

According to equation (3), if the angular acceleration is zero, the average damping coefficient is:

$$a_2 = M/\dot{\theta} = 0.032$$

The a_2 for backward motion is about 0.019.

System identification

Although a_1, a_2 can be obtained through direct parameter measurement and computation, the inaccuracy of direct parameter measurement and the sensitive component to the bias error (especially for a_2, which is computed from damping friction and angular speed) may result in significant parameter error. Impulse response also failed to generate consistent results for damping analysis due to the electrical characteristics (e.g. rising time and torque saturation) of amplifier board and motor.

In order to get more accurate model parameters, the system identification approach is used in this paper to determine the model parameters. The directly measured parameters are used as the starting point for system identification process and a baseline for model validation.

Setup

The parameters to be estimated are a_1, a_2 in equation (3).

For the model of equation (3), define $X = \dot{\theta}$, $u = M$ and $Y = X$, we have:

$$\begin{cases} \dot{X} = AX + Bu \\ Y = CX \end{cases}$$

where, $A = -a_2/a_1$; $B = -1/a_1$; $C = 1$.

By measuring the motor torque data (to compute M) and track encoder data (to compute $\dot{\theta}$), we may estimate the model parameters A and B (hence a_1, a_2). A number of track torque and motion data (forward, backward, short/long distance) were recorded for system identification and a set of

suitable average parameters were computed as model parameters.

Procedure

MatLab utilities are used for system identification. First, motor torque (M_m) and motor angle (θ) is recorded from actual robot motions, then the actual input data M and actual output data $\dot{\theta}$ are computed from the motor torque and angle. Applying the actual input/output data and initial parameters (get from direct measurement in the third section) to the system identification model generates the best-estimated model parameters.

After parameter estimation, the model output data are compared with the actual output data for validation. The validation utilizes both system identification input data and some random selected input data to generate model outputs for comparison.

Data and results

The system identification is done mainly using data recorded from application's motion data. A number of motion data with different travel distance were collected and used for system identification. The final estimated parameters were determined by averaging these system identification results. Described below is one sample result with system identification.

Data for system identification

An end-to-end track motion is used for data collection. The track moving distance is about 17.5 in. in backward direction. The theta (θ) and torque (M_m) data were recorded with a sampling rate of 250 Hz. A portion (100 points) of the computed theta speed ($\dot{\theta}$) and torque data plots is shown in Figure 6.

The following system parameters are generated by system identification using PEM function in MatLab (The function PEM provides unbiased estimation method):

$$a_1 = 0.028, \quad a_2 = 0.0057$$

The system parameters based on direct measurement are:

$$a_1 = 0.029, \quad a_2 = 0.019 \ \text{(backward motion)}$$

Figure 6 Raw data for system identification

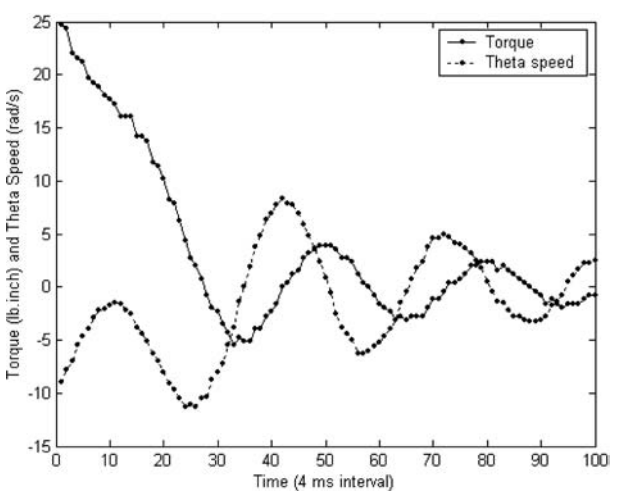

Obviously there is a significant difference between system identification result and direct measurement in a_2. The main reason for this is due to the usage of the average motor torque and static friction for the computation of the direct measurement parameter. The static friction value has a significant impact on a_2 computation. In some locations (e.g. backward motion in track location 12.2 in.), the static friction can be as big as 0.855 (lb in.), which results in a a_2 value about 0.0058 (quite close to the system identification result). Other reasons for the discrepancy between the direct measurement and system identification result are inaccurate torque measurement, model simplification, non-linearity and the rigid body assumption (the belt spring impact is not considered).

Validation

To verify the system identification results, the model outputs from both system identification input data and random selected input data were compared with the actual outputs. In both validations, $\dot{\theta}$ data is used for comparison. The left plots of Figure 7 shows the model output and the actual output of $\dot{\theta}$ (Y-axis in rad/s) vs time (X-axis in second) driven by the input data recorded for system identification.

The right plots of Figure 7 shows the model output and the actual output driven by a random selected input data.

In order to quantitatively investigate the modeling error, the model output errorindex (EI) is defined to compare the fitting of model output and actual output:

$$\text{EI} = \frac{\sqrt{\sum(\text{model output} - \text{actual output})^2}}{\sqrt{\sum \text{actual output}^2}}$$

where Σ is for all the given data points.

Obviously, the EI describes how closely the model output follows the actual output in overall perspective. If model outputs are the same as actual outputs, the EI is 0. If the error between model outputs and actual outputs is the same absolute value as actual output in every data point, the EI is 1.

Table II shows the EI results from Figure 7 and a few different types of input data. In all the cases, the model outputs closely follow the actual outputs, which confirm that the model is a good approximation of the real robot track plant. The variation between the model output and actual output may be due to the belt impact, uneven static friction, and inaccurate torque measurement.

Root-cause analysis

The root *locus* approach is utilized for root-cause and PID tuning analysis. Figure 8 shows the root *locus* with the given model. The blue (black) curve shows how close loop poles change with KP and KD. The red square shows close loop poles with the current PID parameters.

By using root *locus* utility, we can easily investigate the impact of PID parameter (KP and KD) on damping ratio and natural frequency, which are related to track vibration amplitude and tracking error. Some findings using root *locus* approach are summarized below:

- The track system is extremely under-damped with the current parameters. The damping ratio is about 0.16. The two dominant poles are far from the critical damping ratio region (damping ratio: 0.707). This is the root-cause of the vibration.

Figure 7 Model output and actual output comparison

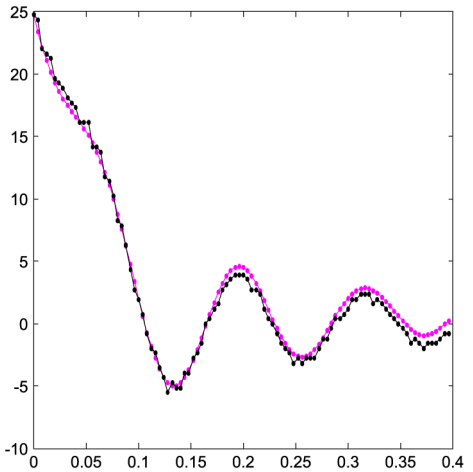

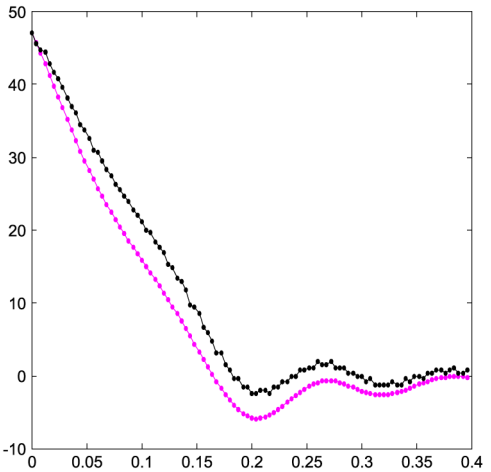

Table II Model output EI with different input data

Test case	Test description	EI value
1	Input data for system identification in Figure 7	0.047
2	Random S-curve input data in Figure 7	0.182
3	Track move 12 in.	0.191
4	Track move 24 in.	0.196

Figure 8 Analysis using root *locus* approach trajectory generator

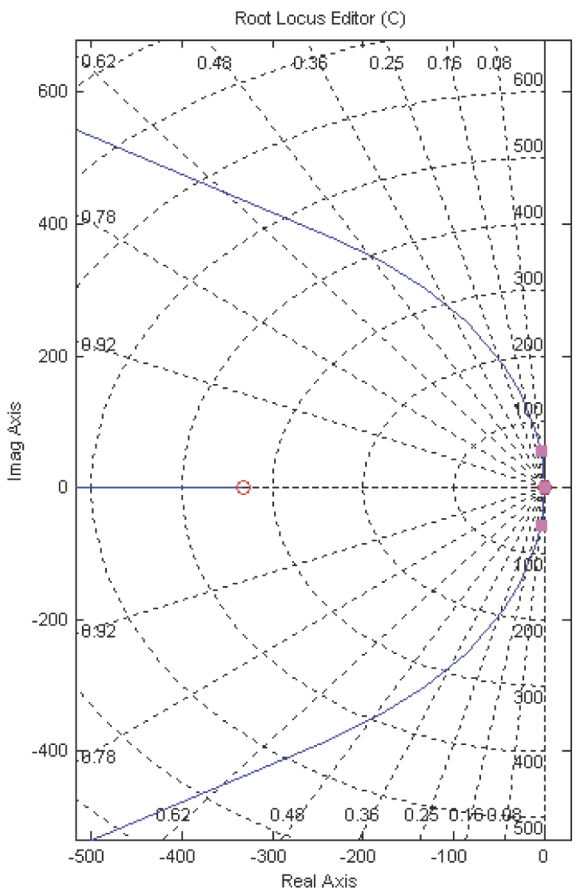

- Though the damping ratio can be improved by increasing the KD or decreasing the KP (either or both), the tuning subjects to certain constraints (e.g. decreasing KP subjects to the tracking error limit and increasing KD subjects to electrical noise). It is impossible to tune the PID parameter to critical damping ratio under current system constraints.

In the track model of Figure 3, we may input the actual commanded position data and output the motor angle (or track displacement if needed), and then compare the model simulation output with the actual output. The comparison showed that the model output is fairly close to the actual output, which further proves the validity of the model and verifies that the current PID control is not able to eliminate the vibration even with S-curve on.

The solution for vibration suppression

According to the system structure and vibration root-cause analysis, the track vibration is due to insufficient damping of the track system. A suitable solution is required to resolve this problem.

The proposed solution in this paper takes two major considerations into account. First, redesign of the controller (e.g. use model-based control approaches or add in filters) or robot hardware involves substantial resources and cost, which is not feasible in this application. Second, increasing damping through PID tuning is subjected to system constraints, which cannot achieve desired performance improvement. A practical industrial solution has to be both easy to implement and able to provide consistent, reliable and significant performance improvement. To seek such a solution, this paper focuses on improving the trajectory generation such that the trajectory generator will not excite unacceptable vibrations.

In order to resolve the vibration problem, an acceleration smoother is proposed in this paper in addition to the conventional PID tuning. Figure 9 shows the diagram of the acceleration smoother and PID controller. This acceleration smoother is embedded in the commanded position (trajectory) generator, which does not involve a redesign of the controller. The testing results showed good improvement and negligible side effects.

Figure 9 The solution for vibration suppression

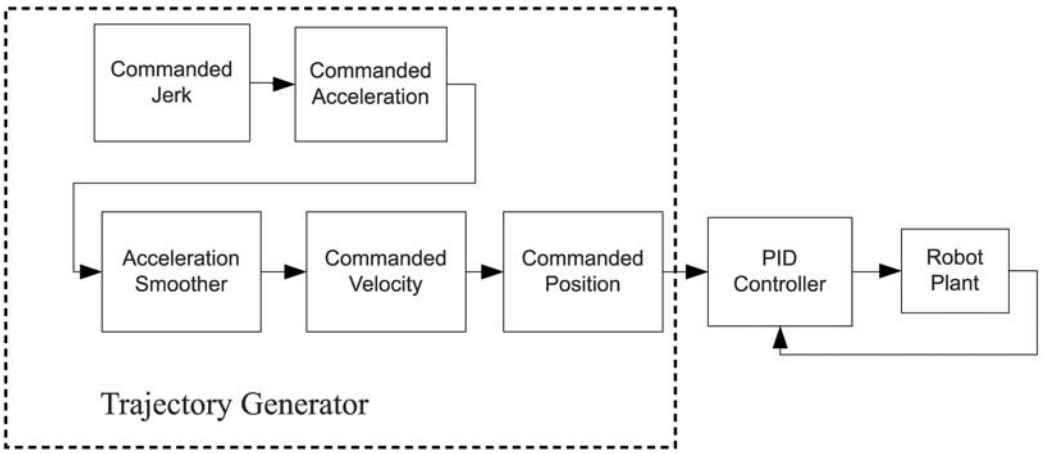

The root *locus* analysis showed that the current damping ratio of the system is not sufficient. By decreasing the proportional gain (KP) and increasing the derivative gain (KD), we are able to increase the damping ratio of the close loop system. However, PID tuning is limited by tracking error and electrical noise in the amplifier board. A new set of PID parameters was proposed based on the guidance from the root *locus* utility. The new parameters set the current KP, KI and double the KD (KP = 320, KI = 1.5, KD = 1.92) for the application. Limited performance improvement by PID tuning is shown in Table II.

Acceleration smoother in trajectory generator

To further improve the vibration suppression performance, which PID tuning failed to achieve, an acceleration smoother is proposed to provide a smooth motion profile. By eliminating the abrupt change in the acceleration/deceleration, a smoother commanded trajectory is generated, which in the end results in substantial vibration reduction at the end-effector.

The most popular conventional S-curve motion profile in industries is the third order trajectory generator with abrupt transitions in the acceleration/deceleration and the jerk (shown in Figure 10). The original track trajectory generator uses a third order S-curve motion profile.

In Figure 10, "j" is commanded jerk, "a" is commanded acceleration; "v" is commanded velocity and "x" is commanded position. In this case, changing the "j" value will make change of the acceleration ramp. However, adjusting j will not eliminate the sharp transitions in acceleration/deceleration and hence will not be able to significantly reduce the vibration unless the j is substantially small resulting in substantially slow motion.

The idea of digital acceleration smoother is to smooth the sharp transitions in acceleration/deceleration to reduce the vibration without substantially extending motion time. As shown in the acceleration plot in Figure 10, the sharp transition corners are eliminated by the smooth transition curves (see the acceleration plots before/after smoothing).

The digital acceleration smoother is actually a first order filter modeled as:

$$\frac{U_o(Z)}{U_i(Z)} = \frac{z}{z - e^{-(T/\tau)}}$$

where U_o is the commanded acceleration output; U_i is the commanded acceleration input; T is the sampling time interval and τ is the time constant.

The time constant τ is to be designed to provide the desired performance. Selecting τ is a trade off between smoothness and speed. Currently it is set to 0.05 s to achieve significant vibration reduction without much impact on throughput.

Distinguished features of the acceleration smoother

The acceleration smoother can effectively reduce the vibration by smoothing out the acceleration/deceleration (hence to provide a smoother motion profile).

There are two major differences between the proposed acceleration smoother and the conventional first order low pass filter. First, the acceleration smoother is not used for filtering the sensor output or reducing the control output jitter. It is used for smoothing the commanded acceleration of

Figure 10 Third order trajectory generator and acceleration smoother

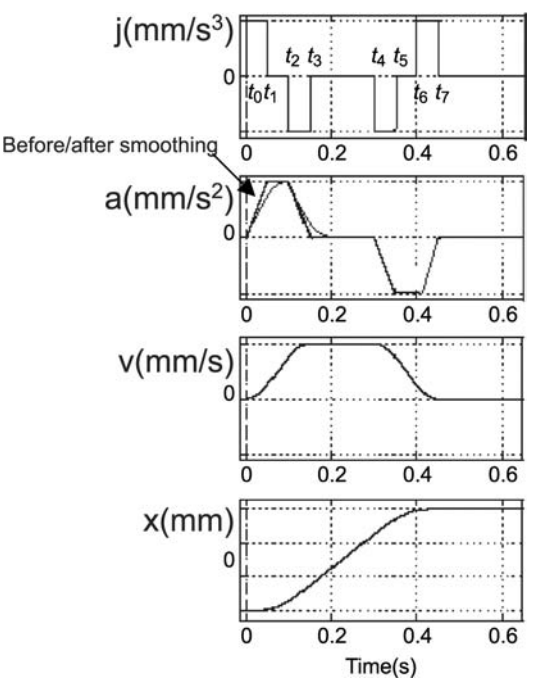

the trajectory generator. Second, the acceleration smoother is not located behind the sensor module or in the control loop. It is located inside the trajectory generator. So its implementation does not require redesign of the controller or robot.

There are two major advantages for the acceleration smoother comparing to the multi-order S-curve motion profile (e.g. the fourth order trajectory generator in Lambrechts *et al.*, 2004). First, the acceleration smoother leads to a velocity profile with infinite order of smoothness (i.e. no abrupt transition in any order of its derivative); second, it is much easier to implement.

Experimental test results

Improvement in vibration amplitude

Two robot tracks were tested with separate PID tuning and acceleration smoother. The vibration amplitude, which is defined as the maximum peak-to-peak amplitude of robot's vibration starting from motion completion time, is used to evaluate the vibration suppression performance.

Significant improvements were observed in both robot tracks. Table III shows the average results from five motion tests comparing PID and acceleration smoother (ORG is original PID parameter, no acceleration smoother). New PID parameters resulted in approximately 23 percent improvement in vibration amplitude. The acceleration smoother resulted in about 45 percent improvement in vibration amplitude.

Impact on throughput and repeatability

Smothering acceleration/deceleration may cause longer commanded motion time. For a typical track motion and the given time constant of the acceleration smoother, there is a 3.45 percent increment in the commanded motion completion time, which will theoretically lead to a throughput loss of about 0.19 percent in a typical application (or 7.1 s/h, assuming the tool throughput is 120 wafers/h). However, the actual motion completion time is less due to shorter settling time resulting from the quickly decayed vibration. Further more, any throughput loss can be avoided by increasing the maximum commanded acceleration and speed value, which are no longer limited by the original vibration performance.

Testing with a laser repeatability fixture on two robots showed that 24-53 percent improvements in range and 3-sigma value were achieved.

Table III Average improvements on vibration amplitude

	1		2	
Track no.	Max vibration amplitude (mm)	Improvement (percent)	Max vibration amplitude (mm)	Improvement (percent)
ORG	1.35	0.0	0.79	0.0
New PID	1.02	24.4	0.62	21.5
AC smoother	0.71	47.4	0.44	44.3

Conclusions

This paper presents a mathematical model for an industrial robot track and a model-based vibration analysis. A feasible solution using acceleration smoother is proposed and presented for vibration suppression. The test results showed substantial performance improvements in vibration suppression.

The robot track is used for wafer handling in semiconductor manufacturing and bio-chip fabrication industries. The root-cause analysis and vibration suppression solution proposed in this paper effectively resolved an industrial problem. Consistent performance improvement in real systems with varied system characteristics has been achieved.

The current design of the acceleration smoother is mainly empirical based. An interesting research topic is to find a systematic way for optimal or sub-optimal design.

References

Book, W.J., Maizza-Neto, O. and Whitney, D.E. (1976), "Feedback control of two beam, two joint systems with distributed flexibility", *Journal of Dynamic Systems, Measurement, and Control*, Vol. 97 No. 4, pp. 424-31.

Coyle-Byrne, J. and Klafter, R.D. (1990), "Real-time zone-adaptive control of SCARA-type robot arm", *Proceeding of ICRA 1990*, Vol. 3, pp. 2089-94.

Doyle, J.C., Glover, K., Khargonekar, P.P. and Francis, B.A. (1989), "State-space solutions to standard H_2 and H_∞ control problems", *IEEE Transaction of Automation and Control*, Vol. 34 No. 8, pp. 831-47.

Kim, N. and Hong, M. (2004), "Diagnosis and reduction of robot arm vibration for 12-inch wafer spin scrubber", *Key Engineering Materials*, Vols 270-273, pp. 884-9.

Lambrechts, P., Boerlage, M. and Steinbuch, M. (2004), "Trajectory planning and feed forward design for high performance motion systems", *Proceedings of American Control Conference*, pp. 4637-42.

McEver, M.A. and Leo, D.J. (2001), "Autonomous vibration suppression using on-line pole-zero identification", *ASME Journal of Vibration and Acoustics*, Vol. 123 No. 4, pp. 487-95.

Meckl, P.H. and Seering, W.P. (1985), "Minimizing residual vibration for point-to-point motion", *Journal of Vibration and Acoustics*, Vol. 107, pp. 378-82.

Murphy, B.R. and Watanabe, J. (1992), "Digital shaping filters for reducing machine vibration", *IEEE Transaction on Robotics and Automation*, Vol. 8 No. 2, pp. 285-9.

Piazzi, A. and Visioli, A. (2000), "Minimum-time system inversion based motion planning for residual vibration reduction", *IEEE/ASME Transactions on Mechatronics*, Vol. 5, pp. 12-22.

Roy, J. and Whitcomb, L.L. (1999), "Comparative structural analysis of 2-dof semi-direct-drive linkages for robot arms", *IEEE/ASME Transactions on Mechatronics*, Vol. 4 No. 1, pp. 82-6.

Singer, N.C. and Seering, W.P. (1990), "Preshaping command inputs to reduce system vibration", *ASME Journal of Dynamic Systems, Measurement, and Control*, Vol. 112, pp. 76-82.

Singhose, W. and Singer, N. (1996), "Effects of input shaping on two-dimensional trajectory following", *IEEE Transactions on Robotics and Automation*, Vol. 12, pp. 881-7.

Singhose, W., Seering, W. and Singer, N. (1994), "Residual vibration reduction using vector diagrams to generate shaped inputs", *ASME Journal of Mechanical Design*, Vol. 116, pp. 654-9.

Whitcomb, L.L., Rizzi, A.A. and Koditschek, D.E. (1993), "Comparative experiments with a new adaptive controller for robot arms", *IEEE Transactions on Robotics and Automation*, Vol. 9, pp. 59-70.

Corresponding author

WeiMin Tao can be contacted at: david.tao@sbcglobal.net